Catalysis Science & Technology

PAPER

Cite this: *Catal. Sci. Technol.*, 2017, 7, 650

Double-active site synergistic catalysis in Ru–TiO_2 toward benzene hydrogenation to cyclohexene with largely enhanced selectivity†

Xiaoge Xue,‡[a] Jie Liu,‡[b] Deming Rao,[a] Simin Xu,[a] Weihan Bing,[a] Bin Wang,[c] Shan He*[a] and Min Wei*[a]

Received 25th November 2016,
Accepted 4th January 2017

DOI: 10.1039/c6cy02471h

www.rsc.org/catalysis

The selective hydrogenation of benzene is one promising route to obtain cyclohexene, a key intermediate for the production of various value-added fine chemicals. Herein, we report the preparation of a novel Ru/TiO_2 catalyst encapsulated by a porous TiO_2 coating (denoted as (Ru/TiO_2)@*p*-TiO_2) for this reaction, in which the supported Ru particles serve as active sites for hydrogen dissociation while the porous TiO_2 surface acts as the active center for benzene hydrogenation. By virtue of the shielding effect of the porous TiO_2 layer with a suitable pore size, only hydrogen molecules can diffuse into the interior Ru surface for dissociation adsorption, followed by hydrogen spillover from Ru to the porous TiO_2 surface and subsequent hydrogenation of adsorbed benzene there. Cyclohexene temperature programmed desorption (CHE-TPD) and DFT calculations demonstrate that cyclohexene shows a more beneficial desorption and a much higher activation energy for its further hydrogenation over the TiO_2 surface in comparison with the Ru surface, accounting for the largely enhanced catalytic performance (benzene conversion: 98.1%, cyclohexene selectivity: 76.6%). This double-active-site synergistic catalysis, to the best of our knowledge, gives the highest cyclohexene yield ever reported.

1. Introduction

The partial hydrogenation of benzene offers a cost-effective and atom-economical route for the production of cyclohexene—a key intermediate for various value-added fine chemicals.[1,2] Ruthenium-based catalysts have been widely used in this hydrogenation conversion but still show limited selectivity to cyclohexene due to the thermodynamically favorable deep hydrogenation reaction.[3] Great efforts have been focused on the modulation of hydrophilicity[4–6] and electronic structure[7–9] of ruthenium catalysts, so as to achieve facile desorption of cyclohexene and inhibit further hydrogenation in such a consecutive hydrogenation process. However, to date, how to precisely control the one-step hydrogenation of benzene over Ru-based catalysts is still an arduous assignment and needs a deep investigation.

In a heterogeneous catalytic hydrogenation reaction, dissociation of hydrogen molecules and subsequent hydrogenation of reactants on active sites are two key steps in determining catalytic performance.[10] Regarding the selective hydrogenation of benzene over a supported Ru catalyst, the active sites on the surface of Ru not only dissociate hydrogen molecules to give active hydrogen species but also catalyze the hydrogenation conversion of adsorbed benzene. This one-active center-dependent catalysis would result in a high concentration of surface dissociated hydrogen, which facilitates the deep hydrogenation of cyclohexene to cyclohexane. Moreover, the low activation energy of deep hydrogenation over metallic Ru may accelerate this process, which has been observed in other hydrogenation reactions.[11] It is reported that some supports (*e.g.*, TiO_2,[12] ZrO_2 (ref. 13) and CeO_2 (ref. 14)) can also catalyze the conversion of benzene *via* the well-known spillover hydrogen effect, serving as the supplementary/subordinate active center for hydrogenation.[15] This inspires us to explore a two-active center-dependent catalysis approach: if the hydrogen dissociation center (Ru) and benzene hydrogenation center (support) are separately located in geometric space, the hydrogenation of benzene would occur *via* the spillover hydrogen mechanism. This new catalytic approach would control the concentration of active hydrogen species at

[a] *State Key Laboratory of Chemical Resource Engineering, Beijing Advanced Innovation Center for Soft Matter Science and Engineering, Beijing University of Chemical Technology, Beijing 100029, P. R. China. E-mail: vh30@163.com, weimin@mail.buct.edu.cn*

[b] *SINOCHEM Quanzhou Petrochemical Co., Ltd., Quanzhou 362103, P. R. China*

[c] *Beijing Research Institute of Chemical Industry, Sinopec Group, Beijing 100013, P. R. China*

† Electronic supplementary information (ESI) available. See DOI: 10.1039/c6cy02471h

‡ These authors contributed equally to this work and should be considered as co-first authors.

a moderate level; furthermore, the activation energy of deep hydrogenation of cyclohexene over a metal oxide support is much higher than that over Ru, both of which would facilitate the desorption of cyclohexene and thus enhance the hydrogenation selectivity.

Herein, we prepare a novel Ru/TiO_2 catalyst encapsulated by a porous TiO_2 layer (denoted as $(Ru/TiO_2)@p\text{-}TiO_2$) *via* a facile two-step procedure: hydrothermal deposition of the titania layer on the surface of Ru/TiO_2, followed by the removal of the pore generator to produce a porous TiO_2 coating on Ru/TiO_2 (Scheme 1). TEM measurements show that the Ru/TiO_2 particles are coated by an amorphous-like, porous TiO_2 layer, which can specifically allow the diffusion of hydrogen molecules other than benzene as revealed by the TPD technique. The as-synthesized $(Ru/TiO_2)@p\text{-}TiO_2$ catalyst exhibits a surprisingly high selectivity toward benzene hydrogenation (benzene conversion: 98.1%; cyclohexene selectivity: 76.6%), which is the highest cyclohexene yield to the best of our knowledge. FTIR spectra demonstrate that spillover hydrogen from the metallic Ru transforms to active hydroxyl species on the surface of the TiO_2 coating, which then participates in the hydrogenation of benzene adsorbed there. DFT calculations reveal that TiO_2 both accelerates the desorption of cyclohexene and exerts a higher energy barrier for deep hydrogenation compared with metallic Ru. This double-active center-dependent approach over the $(Ru/TiO_2)@p\text{-}TiO_2$ catalyst takes the advantages of $Ru–TiO_2$ synergistic catalysis, which results in the largely enhanced selectivity to cyclohexene.

2. Experiment section

2.1 Materials

$RuCl_3{\cdot}3H_2O$, TiO_2 (anatase), tetra-*n*-butyl titanate (TnBT), tetradecyl trimethyl ammonium bromide (TTAB), ethanol, benzene, cyclohexene and cyclohexane were purchased from Sigma-Aldrich and used without further purification. Deionized water was used in all the experimental processes.

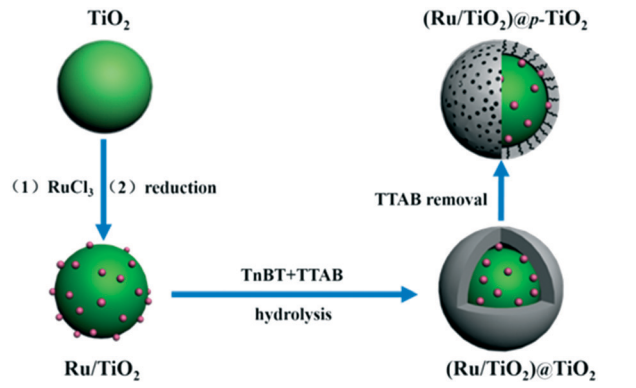

Scheme 1 Schematic illustration for the synthesis of the porous TiO_2-capped Ru/TiO_2 catalyst.

2.2 Preparation of catalysts

Preparation of TiO_2 supported Ru particles (Ru/TiO_2). TiO_2 (4.0 g) was dried overnight in an oven at 100 °C and dispersed in a $RuCl_3{\cdot}3H_2O$ aqueous solution (0.1643 g, 300 mL) with ultrasonication, followed by vigorous stirring for 3 h. The obtained suspension was separated by centrifugation, washed with deionized water until no Cl^- was detected by the $AgNO_3$ reagent, and then dried in an air circulating oven at 60 °C for 12 h. Subsequently, the sample was reduced in 10% H_2 (H_2/N_2 = 1 : 9, v/v) at 400 °C for 3 h with a heating rate of 5 °C min^{-1}, yielding TiO_2 supported Ru particles (denoted as Ru/TiO_2).

Preparation of porous TiO_2 coated Ru/TiO_2 ($(Ru/TiO_2)@p\text{-}TiO_2$). Coating of the porous TiO_2 layer onto Ru/TiO_2 particles was carried out by a reported method with some modification.[16] In detail, 1.0 g of Ru/TiO_2 and 1.0 g of TTAB were added into 500 mL of ethanol solution (ethanol/H_2O = 4 : 1, v/v). After agitation with vigorous ultrasonication for 3 h, 100 mL of ethanol solution containing 0.2 g of TnBT was added dropwise into the above suspension under vigorous stirring and the resulting mixture was aged at room temperature for 3 h. Subsequently, the obtained suspension was filtered and dried under vacuum at 50 °C for 12 h to yield the $(Ru/TiO_2)@TiO_2$ sample. Finally, the as-synthesized sample was calcined at 450 °C in air to produce a porous TiO_2 coating by the removal of the TTAB surfactant, resulting in the $(Ru/TiO_2)@p\text{-}TiO_2$ sample.

2.3 Catalytic evaluation

Prior to the catalytic evaluation, the $(Ru/TiO_2)@p\text{-}TiO_2$ catalyst was first pretreated in a gaseous mixture of H_2/N_2 (1/9, v/v) for 1 h with a total gas flow of 100 mL min^{-1} at 400 °C with a heating rate of 5 °C min^{-1} and then was evaluated by selective hydrogenation of benzene according to the same procedure reported in our previous work.[21]

2.4 Characterization

The temperature programmed desorption of hydrogen and carbon monoxide (H_2/CO) was conducted on a Micromeritics ChemiSorb 2920. Before desorption measurements, the sample was pretreated at 400 °C in a gaseous mixture of H_2 and Ar (1 : 9, v/v) for 2 h and then cooled down to room temperature. H_2/CO was introduced for 1 h. Subsequently, the sample was purged with carrier gas (argon for H_2-TPD; helium for CO-TPD) for the removal of physisorbed species, followed by the TPD process in a carrier gas stream at a rate of 50 mL min^{-1} and a temperature ramp of 10 °C min^{-1}.

The temperature programmed desorption of cyclohexene (CHE-TPD) was conducted on a Micromeritics ChemiSorb 2920. The sample was first pretreated at 400 °C in a gaseous mixture of H_2 and He (1 : 9, v/v) for 2 h, cooled down to room temperature, and then cyclohexene vapor was introduced until adsorption saturation. Subsequently, the sample was purged with helium for the removal of

physisorbed species, followed by the TPD process in a carrier gas stream at a rate of 40 mL min^{-1} and a temperature ramp of 10 °C min^{-1}.

Fourier-transformed infrared absorption spectra were obtained using a Nicolet 380 instrument spectrophotometer. The nature of the acid sites was characterized by FTIR spectroscopy of adsorbed pyridine (Py-IR). The sample (20 mg) was pressed into a wafer of 1.3 cm diameter, installed in an IR cell with a CaF_2 window, reduced at 400 °C for 3 h, followed by evacuation treatment at this temperature. Subsequently, the sample was cooled to 150 °C for recording the background spectrum. With the introduction of pyridine into the cell for 2 h, the spectrum was recorded with an accumulation of 32 scans after the removal of physisorbed pyridine by evacuation treatment. The amount of Lewis acid sites involved in the adsorbed pyridine (n_{Py}) was calculated based on the following equation:

$$n_{Py} = 1.42A \times R^2/m \quad (1)$$

where A, R and m are the surface area (cm^{-2}), radius (cm) and weight (g) of the sample wafer. In addition, to gain insight into the process of spillover hydrogen-based benzene hydrogenation on the surface of TiO_2, *in situ* FTIR spectra recorded on the Ru/TiO_2@*p*-TiO_2 sample were obtained. In detail, the sample (20 mg) was pressed into a wafer and evacuated at 400 °C in the same cell. After the background spectra at different temperatures (400, 300, 200, 150, 100 °C and RT) were recorded, the sample was treated by temperature programmed reduction with simultaneous collection of FTIR spectra. For *in situ* FTIR measurements, the sample of Ru/TiO_2@*p*-TiO_2 was pretreated in H_2 at 150 °C. As a reference, the same sample was pretreated under vacuum at 150 °C. After the background spectra of these two samples at 150 °C were recorded, the benzene steam was introduced into the two quartz cells simultaneously for the collection of FTIR spectra at 150 °C.

2.5 Computational methods

The Ru(001) and TiO_2(101) surfaces were represented as a four-layer slab with a p(4 × 4) supercell. Only the bottom atoms of the slab were constrained to their crystal lattice positions; the neighboring slabs were separated in the direction perpendicular to the surface with a vacuum region of 15 Å. Transition state (TS) searches were performed at the same theoretical level with the NEB method, followed by obtaining the true saddle point with a unique negative frequency. To study the interaction between the Ru surface and cyclohexene, the adsorption energy of cyclohexene (E_{ads}) was calculated according to the following equation:

$$E_{ads} = E(\text{facet}) + E(\text{cyclohexene}) - E(\text{facet with cyclohexene}) \quad (2)$$

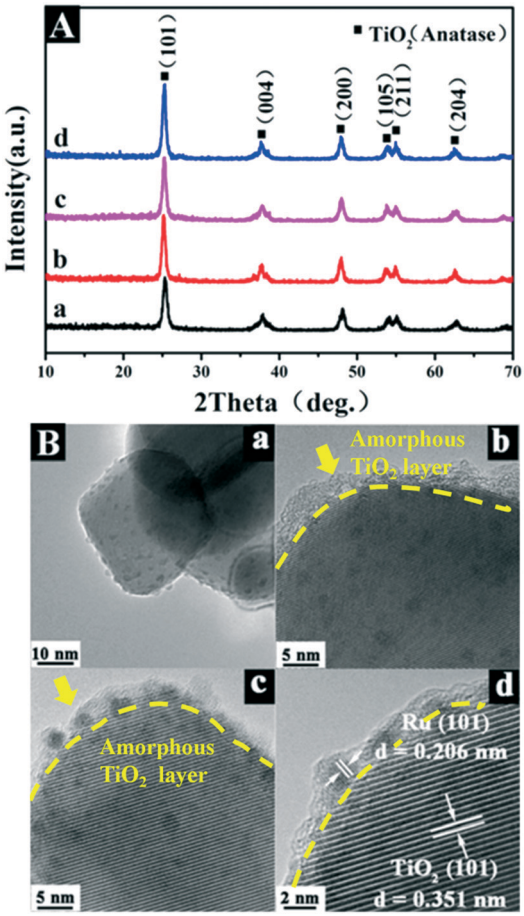

Fig. 1 (A) XRD patterns of (a) TiO_2, (b) Ru/TiO_2, (c) (Ru/TiO_2)@TiO_2 and (d) (Ru/TiO_2)@*p*-TiO_2. (B) HRTEM images of (a) Ru/TiO_2, (b) (Ru/TiO_2)@TiO_2, and (c and d) (Ru/TiO_2)@*p*-TiO_2.

3. Results and discussion

3.1 Structural and morphological studies on catalysts

(Ru/TiO_2)@*p*-TiO_2 was prepared *via* a facile two-step procedure: a titania layer was coated on the surface of Ru/TiO_2 particles, followed by calcination to remove the pore generator to obtain a porous TiO_2 coating on Ru/TiO_2 (Scheme 1). Fig. 1A shows the XRD patterns of bare TiO_2, Ru/TiO_2, (Ru/TiO_2)@TiO_2 and (Ru/TiO_2)@*p*-TiO_2 samples. The diffraction peaks at 2θ = 25.2°, 37.9°, and 48.1° for bare TiO_2 (Fig. 1A-a) are indexed to anatase TiO_2 (JCPDS no. 21-1272). After the immobilization of Ru nanoparticles on TiO_2, the resulting Ru/TiO_2 sample (Fig. 1A-b) shows no obvious change, implying a high dispersion or a low concentration of Ru NPs. In the cases of (Ru/TiO_2)@TiO_2 (Fig. 1A-c) and (Ru/TiO_2)@*p*-TiO_2 (Fig. 1A-d) with a nonporous or a porous TiO_2 coating, they both display a similar anatase TiO_2 phase. Fig. 1B shows the TEM images of Ru/TiO_2, (Ru/TiO_2)@TiO_2 and (Ru/TiO_2)@*p*-TiO_2, respectively. The Ru/TiO_2 sample displays numerous Ru nanoparticles (mean size: ~2.0 nm) with a high dispersion on the surface of TiO_2 (Fig. 1B-a). After a coating treatment, the obtained (Ru/TiO_2)@TiO_2 sample exhibits a clear

core–shell structure in which the Ru/TiO_2 particle is surrounded by an amorphous-like TiO_2 layer (Fig. 1B-b: ~2 nm). The calcination process for the removal of the pore generator leads to a decrease in the thickness of the TiO_2 layer (Fig. 1B-c: ~1.5 nm). The lattice fringe of 0.351 nm in Fig. 1B-d corresponds to the (101) plane of the anatase TiO_2 core.

Removal of the pore generator (TTAB) during the calcination process is of great importance, which endows the exterior TiO_2 layer with a porous structure. IR spectra reveal the absence of alkyl and quaternary ammonium vibrations of TTAB, indicative of the successful removal of this pore generator (Fig. S1†). Furthermore, the porous TiO_2 layer with a suitable pore size is also crucial for the following catalytic evaluation. Carbon monoxide and hydrogen can be used as probing molecules to investigate the micropores by the temperature programmed desorption (TPD) technique. Fig. 2A displays the H_2-TPD profiles of $(Ru/TiO_2)@p\text{-}TiO_2$ and Ru/TiO_2, respectively, both of which exhibit two strong desorption peaks of hydrogen below 650 °C. According to the previously reported investigation, the peak at low temperature is assigned to the desorption of hydrogen from metallic Ru, whereas the one at high temperature is attributed to the desorption of spillover hydrogen on the TiO_2 support.[17,18] CO-TPD profiles of $(Ru/TiO_2)@p\text{-}TiO_2$ and Ru/TiO_2 are shown in Fig. 2B. A remarkable CO desorption peak at 110 °C is observed for the Ru/TiO_2 sample, which is due to the adsorption of CO on metallic Ru. However, no signal is detected for the $(Ru/TiO_2)@p\text{-}TiO_2$ sample. The results indicate that the micropores in the TiO_2 coating only allow the diffusion of hydrogen into the interior Ru nanoparticles but do not permit the diffusion of CO molecules. This is due to the relatively larger dynamic diameter of the CO molecule (0.38 nm) compared to that of the hydrogen molecule (0.29 nm). In other words, the synthesized $(Ru/TiO_2)@p\text{-}TiO_2$ catalyst would show interesting diffusion behavior when employed in benzene hydrogenation reaction, *i.e.*, the hydrogen molecule can enter the interior surface of Ru, while the benzene molecule, with a larger dynamic diameter than CO, is restricted to remain on the surface porous TiO_2 layer (Table 1).

3.2 Catalytic evaluation for selective hydrogenation of benzene

For the hydrogenation reaction of benzene, the catalytic performance of these catalysts was evaluated. It should be noted that the bare TiO_2 and $(Ru/TiO_2)@TiO_2$ show no activity for this reaction, indicating that the single TiO_2 surface cannot accelerate the hydrogenation of benzene. Therefore, the catalytic behavior of $(Ru/TiO_2)@p\text{-}TiO_2$ was evaluated, with Ru/TiO_2 as a reference sample (Fig. 3; reaction temperature: 150 °C; H_2 pressure: 5.0 MPa). For these two catalysts, the benzene content decreases and the cyclohexane content increases progressively in the whole reaction time, while the cyclohexene content increases at first and then tends to decrease along with the reaction time, according to the widely known behavior of consecutive reactions. The Ru/TiO_2 catalyst shows a high hydrogenation activity but a low selectivity: at a benzene conversion of 73.1%, the corresponding cyclohexene selectivity is only 32.6%. In contrast, the $(Ru/TiO_2)@p\text{-}TiO_2$ catalyst has a low hydrogenation activity but a much higher selectivity. Even at a benzene conversion of 98.1%, the

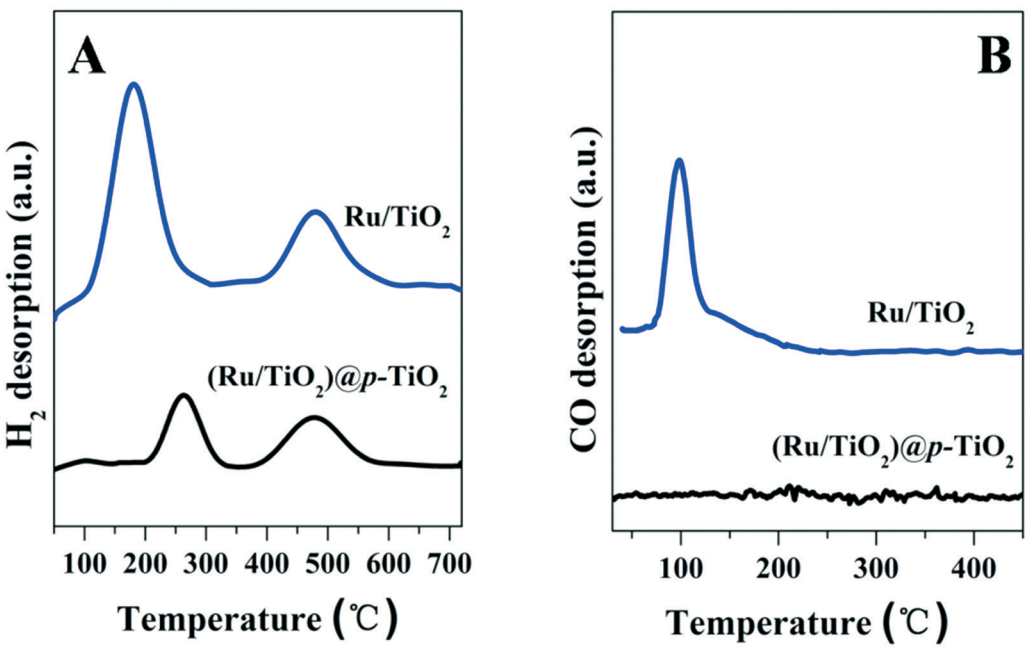

Fig. 2 (A) H_2-TPD and (B) CO-TPD profiles of Ru/TiO_2 and $(Ru/TiO_2)@p\text{-}TiO_2$.

Table 1 Structural parameters of various samples

Samples	Ru[a] (wt%)	Ru dispersion[b] (%)	Mean Ru particle size by TEM (nm)
Ru/TiO_2	1.92	27.5	2.0 ± 0.4
$(Ru/TiO_2)@p\text{-}TiO_2$	1.56	—	2.0 ± 0.5

[a] Values determined by ICP. [b] Values based on the CO-TPD results.

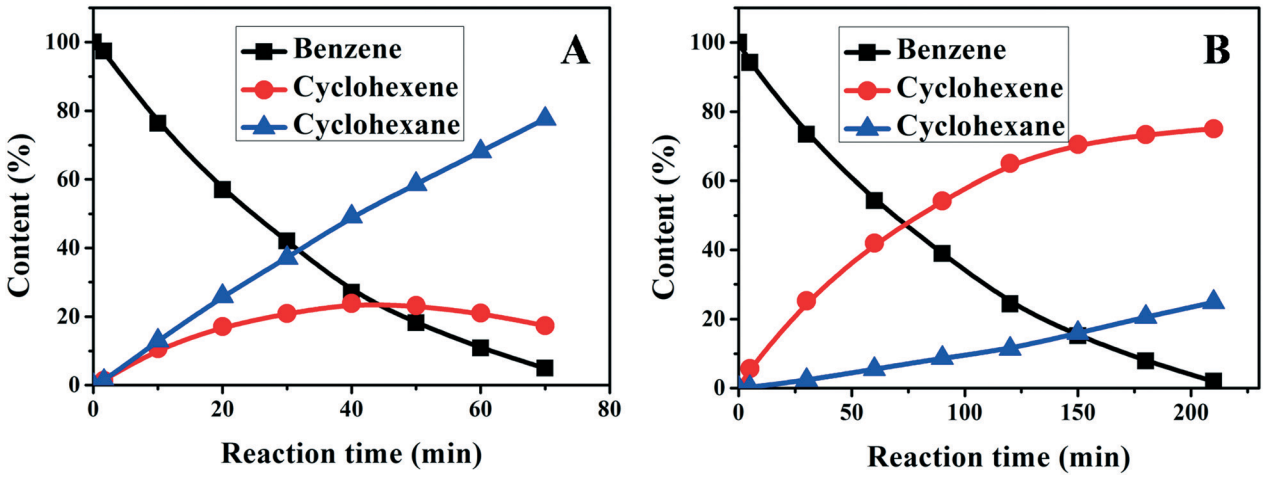

Fig. 3 Time courses of benzene hydrogenation over the (A) Ru/TiO_2 and (B) $(Ru/TiO_2)@p\text{-}TiO_2$ catalysts.

Table 2 Catalytic performance of the Ru/TiO_2 and $(Ru/TiO_2)@p\text{-}TiO_2$ catalysts[a]

Catalyst	t^b (min)	Conv.[b] (%)	S_{CHE}[b] (%)	Y_{CHE}[b] (%)	R_0[c] (mmol s^{-1} g^{-1})
Ru/TiO_2	40.0	73.1	32.6	23.8	3.01
$(Ru/TiO_2)@p\text{-}TiO_2$	210	98.1	76.6	75.1	1.14

[a] Reaction conditions: catalyst, 0.1 g; benzene, 10 mL; H_2O, 20 mL; H_2 pressure, 5.0 MPa; reaction temperature, 150 °C. [b] The results are obtained at the maximum yield of cyclohexene. Conv. = conversion of benzene; S_{CHE} = selectivity to cyclohexene; Y_{CHE} = yield of cyclohexene. [c] Values are calculated based on the amount of converted benzene per minute per gram of catalyst.

selectivity to cyclohexene is still as high as 76.6%. As a result, a maximum cyclohexene yield of 75.1% is obtained over the $(Ru/TiO_2)@p\text{-}TiO_2$ catalyst (Table 2). This is, to the best of our knowledge, the highest value in comparison with the previously reported work (see Table S1†).

Previous reports reveal that the relative hydrogenation rate of benzene to cyclohexene (step 1) is a first-order reaction and cyclohexene to cyclohexane (step 2) is a zero-order reaction.[19,20] Since step 1 and step 2 determine the selectivity to cyclohexene, a relevant kinetic investigation was carried out to examine the effect of the porous TiO_2 coating on the selectivity of benzene hydrogenation. By fitting the reaction data presented in Fig. 3, step 1 and step 2 are identified as first-order and zero-order reactions, respectively (Fig. 4). Based on the slope of the relative kinetic plots, the two rate constants k_1 and k_2 are calculated and listed in Table 3. It can be seen that both k_1 and k_2 for the Ru/TiO_2 catalyst are larger than those of the $(Ru/TiO_2)@p\text{-}TiO_2$ catalyst. In particular, the value of k_2 for the former catalyst reaches up to 120×10^{-2} mol L^{-1} min^{-1}, much higher than that for the latter one (10.4×10^{-2} mol L^{-1} min^{-1}). The results imply that a higher hydrogenation activity of the Ru/TiO_2 catalyst, on the other hand, also brings a faster deep hydrogenation of cyclohexene. As listed in Table 3, the ratio of k_1/k_2 for $(Ru/TiO_2)@p\text{-}TiO_2$ is 0.118 L mol^{-1}, which is 4 times larger than that for the Ru/TiO_2 catalyst, indicating that the deep hydrogenation of cyclohexene is inhibited effectively on the porous TiO_2-decorated catalyst, in agreement with their catalytic performance mentioned above.

3.3 Studies on the structure–property correlation of $(Ru/TiO_2)@p\text{-}TiO_2$

It has been reported that aromatic compounds can be hydrogenated over metal catalysts supported on acid supports more effectively than on neutral or basic supports.[22] This is because the electron-rich aromatic hydrocarbons

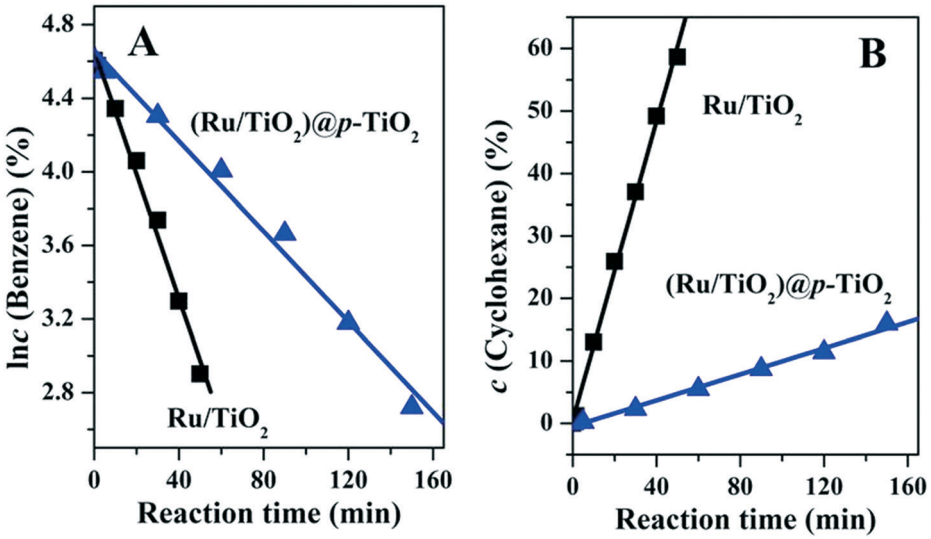

Fig. 4 Plots of (A) ln c (benzene) *vs.* reaction time and (B) c (cyclohexane) *vs.* reaction time over Ru/TiO_2 and $(Ru/TiO_2)@p\text{-}TiO_2$ catalysts, respectively. Reaction conditions: 150 °C, 5.0 MPa.

Table 3 Catalytic kinetic investigation on various Ru-based catalysts

Catalyst	k_1 (10^{-2} min^{-1})	k_2 (10^{-2} mol L^{-1} min^{-1})	k_1/k_2 (10^{-2} L mol^{-1})	Ref.
Ru/TiO_2	3.38	120	2.82	This work
$(Ru/TiO_2)@p\text{-}TiO_2$	1.23	10.4	11.8	This work
$Ru_{1.0}Cu_{0.5}$/MgAl-LDH	2.37	47.2	5.02	21
Ru/B–ZrO_2(1/15)	5.2	108	4.8	3

tend to adsorb on the Lewis acid sites of the support, followed by catalytic hydrogenation with the so-called "spillover hydrogen" that originates from the dissociated hydrogen species on the active metal. Titanium dioxide (TiO_2), with abundant surface Lewis acid sites,[23] is often used as a support for metal catalysts toward aromatic hydrogenation. As shown in Fig. S2,† both the Ru/TiO_2 and $(Ru/TiO_2)@p\text{-}TiO_2$ catalysts show notable Lewis acid site-coordinated pyridine (L-Py) at 1446 cm^{-1}.[24] With regard to the $(Ru/TiO_2)@p\text{-}TiO_2$ catalyst, the active metal is covered by the porous TiO_2 layer, but benzene adsorbed on the exterior TiO_2 surface is still expected to be hydrogenated by spillover hydrogen from the interior metallic Ru, which will be further discussed in the next section. In order to gain a deep understanding of the formation of spillover hydrogen on the porous TiO_2 surface, in this work, the $(Ru/TiO_2)@p\text{-}TiO_2$ catalyst was characterized by the FT-IR technique under a H_2 atmosphere. Fig. 5A shows that after vacuum treatment followed by H_2 injection, a new absorption band at 3670 cm^{-1} assigned to surface hydroxyl is observed, whose intensity increases at first from RT to 200 °C and then decreases from 200 to 400 °C. According to the previous investigation, this newly formed surface hydroxyl can be attributed to the Ti–O(H)–Ti structure.[25,26] In addition, the surface hydroxyl species shows a maximal concentration in the temperature range of 150–200 °C, which is in accordance with the catalytic reaction temperature mentioned above (150 °C). Fig. 5B further shows the

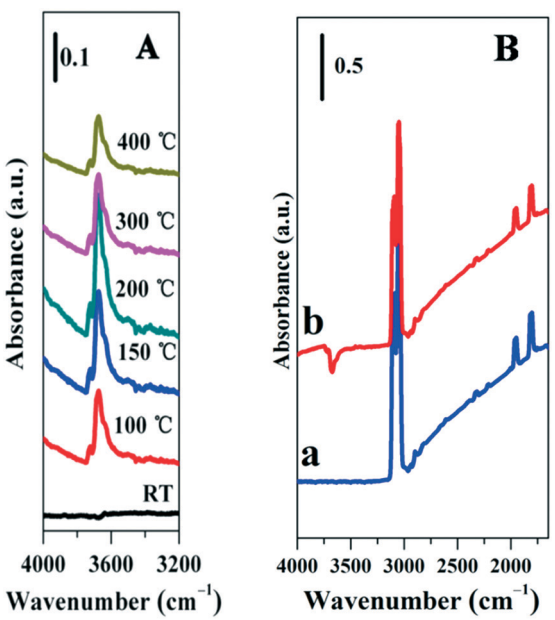

Fig. 5 FT-IR spectra recorded over the $(Ru/TiO_2)@p\text{-}TiO_2$ catalyst: (A) after vacuum treatment at 400 °C followed by H_2 injection at various temperatures; (B) with the introduction of benzene at 150 °C over the fresh catalyst (a) and after H_2 pretreatment (b).

activity test of the surface hydroxyl species by the introduction of benzene. As shown in Fig. 5B-a, when benzene gas was introduced into the quartz cell at 150 °C, a band at 3000–3100 cm^{-1} attributed to the C–H stretching vibration of benzene was observed, indicating the adsorption of benzene on the catalyst surface. After the (Ru/TiO_2)@*p*-TiO_2 catalyst was pretreated in H_2 at 150 °C, benzene gas was introduced into the quartz cell (Fig. 5B-b). It is interesting that a notable negative band at 3670 cm^{-1} is observed, which implies that the hydroxyl species is catalytically active for the hydrogenation of benzene. No obvious signal of the corresponding hydrogenation products (*i.e.*, cyclohexene/cyclohexane) is detected, probably due to their weak adsorption on the catalyst surface. Therefore, the selective hydrogenation of benzene over the (Ru/TiO_2)@*p*-TiO_2 catalyst can be summarized by the following route: the dissociated hydrogen from Ru spills over to the porous TiO_2 surface to form active hydroxyl species, which participates in the hydrogenation of adsorbed benzene.

The hydrogenation activity of the (Ru/TiO_2)@*p*-TiO_2 catalyst is inhibited to some extent, since benzene hydrogenation only occurs on the exterior TiO_2 surface due to diffusion limitation revealed by the H_2/CO-TPD results. Nevertheless, the selectivity of benzene hydrogenation toward cyclohexene is largely enhanced. Based on the structural characterization and *in situ* FT-IR studies, it is concluded that the interior metallic Ru and the porous TiO_2 layer in the (Ru/TiO_2)@*p*-TiO_2 catalyst serve as an independent hydrogen dissociation site and a hydrogenation site, respectively. Therefore, the formation of cyclohexene and its further hydrogenation occur on the surface of TiO_2 rather than on the conventional metallic Ru, which exerts significant influence on the selectivity to cyclohexene in this reaction.

Once cyclohexene is formed on the catalyst surface, it either undergoes desorption or reacts further; the latter outcome would lead to undesirable formation of cyclohexane. In other words, a high selectivity is expected to be obtained over one catalyst that imposes a weak interaction with cyclohexene as well as a high activation barrier for further hydrogenation of cyclohexene. Herein, the interaction between cyclohexene and the catalyst surface was further investigated by temperature programmed desorption measurements of cyclohexene on three representative samples (*i.e.*, pure TiO_2, (Ru/TiO_2)@*p*-TiO_2 and Ru/TiO_2).

It is known that the selectivity of cyclohexene is determined by both the desorption energy of cyclohexene (E_d) and its activation barrier for further hydrogenation (E_a). A lower E_d and a higher E_a are beneficial to enhance the selectivity toward cyclohexene. As displayed in Fig. 6, only one desorption peak of cyclohexene appears at 120 °C for the bare TiO_2 and (Ru/TiO_2)@*p*-TiO_2 catalyst, which is assigned to cyclohexene chemisorbed on the surface of TiO_2. In the case of the Ru/TiO_2 catalyst, besides the same peak at 120 °C, an additional shoulder peak is observed at 180 °C, which is due to the cyclohexene adsorbed on metallic Ru. This result indicates that the desorption of cyclohexene on TiO_2 is easier than that

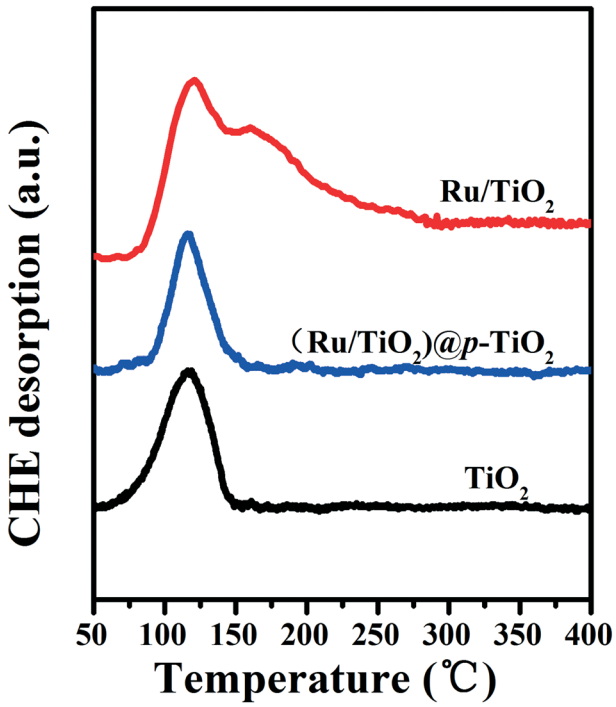

Fig. 6 Cyclohexene temperature programmed desorption (CHE-TPD) profiles over TiO_2, (Ru/TiO_2)@*p*-TiO_2 and Ru/TiO_2, respectively.

on metallic Ru (with an ~60 °C decrease in desorption temperature). The facile desorption behavior of cyclohexene on the (Ru/TiO_2)@*p*-TiO_2 catalyst was also verified by DFT calculations (Fig. S3†): the desorption energy of cyclohexene on the typical $TiO_2(101)$ facet is lower than that on the Ru(001) facet (E_d: 3.56 eV *vs.* 4.30 eV), in agreement with the CHE-TPD results.

DFT calculations were carried out to study the activation barrier for further hydrogenation of cyclohexene (E_a) on typical $TiO_2(101)$ and Ru(001), respectively (Fig. 7). The results show that further hydrogenation of cyclohexene on the $TiO_2(101)$ facet needs a higher activation barrier compared

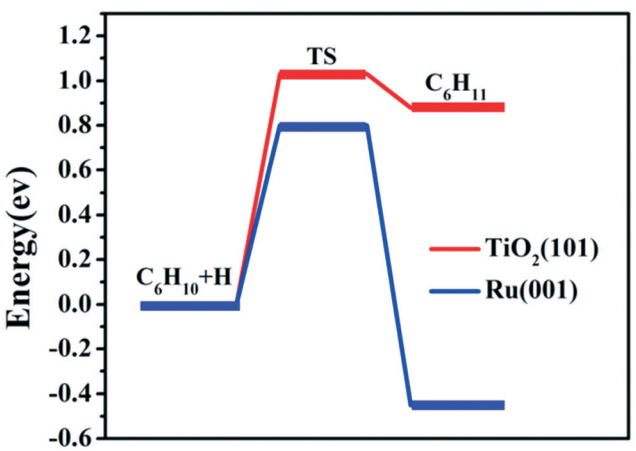

Fig. 7 Energy profiles of the pathways from C_6H_{10} + H to C_6H_{11} on $TiO_2(101)$ and Ru(001), respectively.

with that on the Ru(001) facet (E_a: 1.03 eV *vs.* 0.80 eV). In addition, the process of C_6H_{10} + H to C_6H_{11} on TiO_2(101) is endothermic while that on Ru(001) is exothermic. This indicates that the hydrogenation of cyclohexene on TiO_2 is both kinetically and thermodynamically unfavorable in comparison with that on Ru. Furthermore, based on the adsorption structure of C_6H_{10} + H on the TiO_2(101) facet (Fig. S4a$_1$†), the surface active H species (H_s) tends to interact with the surface oxygen atom in TiO_2, in agreement with the experimental results that dissociated hydrogen spills over to the TiO_2 surface to form active surface hydroxyl (Fig. 5A). Therefore, in the (Ru/TiO_2)@*p*-TiO_2 system with an exterior TiO_2 layer serving as a hydrogenation site, the desorption energy of cyclohexene (E_d) decreases while its activation barrier for further hydrogenation (E_a) increases on the TiO_2 surface, in comparison with those on the Ru surface. This unique hydrogenation approach results in a largely enhanced selectivity toward cyclohexene.

Conclusions

In summary, a porous TiO_2-capped Ru/TiO_2 catalyst was prepared *via* coating titania on the surface of Ru/TiO_2 particles followed by removing the pore generator to produce a porous TiO_2 layer. The interior metallic Ru and the exterior TiO_2 coating in the (Ru/TiO_2)@*p*-TiO_2 catalyst serve as an independent hydrogen dissociation site and a hydrogenation site, respectively. The dissociated hydrogen from Ru spills over to the porous TiO_2 surface to form active hydroxyl species, which participates in the hydrogenation of adsorbed benzene. This unique hydrogenation mode largely facilitates the desorption of cyclohexene and exerts a highly active energy barrier for its further hydrogenation. Consequently, an excellent catalytic performance (benzene conversion: 98.1%; cyclohexene selectivity: 76.6%) was obtained over the (Ru/TiO_2)@*p*-TiO_2 catalyst without the use of any additives. These advantages over conventional catalytic systems make the (Ru/TiO_2)@*p*-TiO_2 catalyst a green and efficient candidate toward selective hydrogenation of benzene.

Acknowledgements

This work was supported by the 973 Program (Grant No. 2014CB932104) and the National Natural Science Foundation of China (NSFC). M. Wei particularly appreciates the financial aid from the China National Funds for Distinguished Young Scientists of the NSFC.

Notes and references

1 H. Nagahara, M. Ono, M. Konishi and Y. Fukuoka, *Appl. Surf. Sci.*, 1997, **121**, 448–451.
2 M. Damm, B. Gutmann and C. O. Kappe, *ChemSusChem*, 2013, **6**, 978–982.
3 G. Zhou, Y. Pei, Z. Jiang, K. Fan, M. Qiao, B. Sun and B. Zong, *J. Catal.*, 2014, **311**, 393–403.
4 J. L. Liu, L. J. Zhu, Y. Pei, J. H. Zhuang, H. Li, H. X. Li, M. H. Qiao and K. N. Fan, *Appl. Catal., A*, 2009, **353**, 282–287.
5 J. Q. Wang, P. J. Guo, S. R. Yan, M. H. Qiao, H. X. Li and K. N. Fan, *J. Mol. Catal. A: Chem.*, 2004, **222**, 229–234.
6 H. Liu, T. Jiang, B. Han, S. Liang, W. Wang, T. Wu and G. Yang, *Green Chem.*, 2011, **13**, 1106–1109.
7 G. Y. Fan, W. D. Jiang, J. B. Wang, R. X. Li, H. Chen and X. J. Li, *Catal. Commun.*, 2008, **10**, 98–102.
8 O. B. Shawkataly, R. Jothiramalingam, F. Adam, T. Radhika, T. M. Tsao and M. K. Wang, *Catal. Sci. Technol.*, 2012, **2**, 538–546.
9 G. Zhou, R. Dou, H. Bi, S. Xie, Y. Pei, K. Fan, M. Qiao, B. Sun and B. Zong, *J. Catal.*, 2015, **332**, 119–126.
10 M. Li, F. Xu, H. Li and Y. Wang, *Catal. Sci. Technol.*, 2016, **6**, 3670–3693.
11 Y. Chen, C. Li, J. Zhou, S. Zhang, D. Rao, S. He, M. Wei, D. G. Evans and X. Duan, *ACS Catal.*, 2015, **5**, 5756–5765.
12 H. Y. T. Chen, S. Tosoni and G. Pacchioni, *ACS Catal.*, 2015, **5**, 5486–5495.
13 E. V. Benvenutti, L. Franken, C. C. Moro and C. U. Davanzo, *Langmuir*, 1999, **15**, 8140–8146.
14 G. Dutta, U. V. Waghmare, T. Baidya and M. Hegde, *Chem. Mater.*, 2007, **19**, 6430–6436.
15 S. Khoobiar, *J. Phys. Chem.*, 1964, **68**, 411–412.
16 W. Li, J. Yang, Z. Wu, J. Wang, B. Li, S. Feng, Y. Deng, F. Zhang and D. Zhao, *J. Am. Chem. Soc.*, 2012, **134**, 11864–11867.
17 S. Velu and S. K. Gangwal, *Solid State Ionics*, 2006, **177**, 803–811.
18 B. Lin, R. Wang, X. Yu, J. Lin, F. Xie and K. Wei, *Catal. Lett.*, 2008, **124**, 178–184.
19 G. Zhou, X. Tan, Y. Pei, K. Fan, M. Qiao, B. Sun and B. Zong, *ChemCatChem*, 2013, **5**, 2425–2435.
20 S. Liu, Y. Guo, X. Yang, Y. Ji and G. Luo, *Chin. J. Catal.*, 2003, **24**, 42–46.
21 J. Liu, S. Xu, W. Bing, F. Wang, C. Li, M. Wei, D. G. Evans and X. Duan, *ChemCatChem*, 2015, **7**, 846–855.
22 S. D. Lin and M. A. Vannice, *J. Catal.*, 1993, **143**, 539–553.
23 K. Hashimoto, Y. Masuda and H. Kominami, *ACS Catal.*, 2013, **3**, 1349–1355.
24 G. Zhou, J. Liu, X. Tan, Y. Pei, M. Qiao, K. Fan and B. Zong, *Ind. Eng. Chem. Res.*, 2012, **51**, 12205–12213.
25 F. Boccuzzi, A. Chiorino, G. Ghiotti and E. Guglielminotti, *Langmuir*, 1989, **5**, 66–70.
26 D. A. Panayotov and J. T. Yates, *J. Phys. Chem. C*, 2007, **111**, 2959–2964.